J|A|C|S ARTICLES

Published on Web 04/08/2009

Liquid-Crystalline Semiconducting Copolymers with Intramolecular Donor−Acceptor Building Blocks for High-Stability Polymer Transistors

Do Hwan Kim,[†] Bang-Lin Lee,*[,†] Hyunsik Moon,[†] Hee Min Kang,[†] Eun Jeong Jeong,[†] Jeong-Il Park,[†] Kuk-Min Han,[†] Sangyoon Lee,[†] Byung Wook Yoo,[†] Bon Won Koo,[†] Joo Young Kim,[†] Wi Hyoung Lee,[§] Kilwon Cho,[§] Hector Alejandro Becerril,[‡] and Zhenan Bao[‡]

Display Laboratory, Materials and Device Institute, Samsung Advanced Institute of Technology, Samsung Electronics Co., Ltd., Yongin 446-712, Korea, Department of Chemical Engineering, Stanford University, 381 North South Mall, Stanford, California 94305-5025, and Department of Chemical Engineering, Pohang University of Science and Technology, Pohang 790-784, Korea

Received December 15, 2008; E-mail: banglin@samsung.com

Abstract: The ability to control the molecular organization of electronically active liquid-crystalline polymer semiconductors on surfaces provides opportunities to develop easy-to-process yet highly ordered supramolecular systems and, in particular, to optimize their electrical and environmental reliability in applications in the field of large-area printed electronics and photovoltaics. Understanding the relationship between liquid-crystalline nanostructure and electrical stability on appropriate molecular surfaces is the key to enhancing the performance of organic field-effect transistors (OFETs) to a degree comparable to that of amorphous silicon (a-Si). Here, we report a novel donor−acceptor type liquid-crystalline semiconducting copolymer, poly(didodecylquaterthiophene-*alt*-didodecylbithiazole), which contains both electron-donating quaterthiophene and electron-accepting 5,5′-bithiazole units. This copolymer exhibits excellent electrical characteristics such as field-effect mobilities as high as 0.33 $cm^2/V \cdot s$ and good bias-stress stability comparable to that of amorphous silicon (a-Si). Liquid-crystalline thin films with structural anisotropy form spontaneously through self-organization of individual polymer chains as a result of intermolecular interactions in the liquid-crystalline mesophase. These thin films adopt preferential well-ordered intermolecular $\pi-\pi$ stacking parallel to the substrate surface. This bottom-up assembly of the liquid-crystalline semiconducting copolymer enables facile fabrication of highly ordered channel layers with remarkable electrical stability.

Introduction

Organic field-effect transistors (OFETs) based on π-conjugated polymers have recently attracted significant attention because of their potential use as soft channel materials in organic/printed optoelectronic devices such as active-matrix flat panel displays (AMFPDs), electronic paper, RFID tags, and chemical/biosensors.[1−8] The solution processability of π-conjugated polymers has also stimulated interest in their utilization as active electronic elements for low-cost, large-area, and flexible active matrix display backplanes, with performance that is comparable to that of hydrogenated amorphous silicon (a-Si:H)-based thin-film transistors.[9−20] However, when polymer-based OFETs are fabricated and tested under ambient conditions,

[†] Samsung Advanced Institute of Technology.
[‡] Stanford University.
[§] Pohang University of Science and Technology.

(1) Dimitrakopoulos, C. D.; Malenfant, P. R. L. *Adv. Mater.* **2002**, *14*, 99.
(2) Ling, M. M.; Bao, Z. *Chem. Mater.* **2004**, *16*, 4824.
(3) Heeger, A. J. *Angew. Chem., Int. Ed.* **2001**, *40*, 2591.
(4) Brabec, C. J.; Sariciftci, N. S.; Hummelen, J. C. *Adv. Funct. Mater.* **2001**, *11*, 15.
(5) Katz, H. E.; Bao, Z.; Gilat, S. L. *Acc. Chem. Res.* **2001**, *34*, 359.
(6) Chabinyc, M. L.; Salleo, A. *Chem. Mater.* **2004**, *16*, 4509.
(7) Fukuda, H.; Ise, M.; Kogure, T.; Takano, N. *Thin Solid Films* **2004**, *464−465*, 441.
(8) Kim, D. H.; Park, Y. D.; Jang, Y.; Yang, H.; Kim, Y. H.; Moon, D. G.; Han, J. I.; Park, S.; Chang, T.; Chang, C.; Joo, M.; Ryu, C. Y.; Cho, K. *Adv. Funct. Mater.* **2005**, *15*, 77.
(9) Bao, Z.; Dodabalapur, A.; Lovinger, A. J. *Appl. Phys. Lett.* **1996**, *69*, 4108.
(10) Lovinger, A. J.; Rothberg, L. J. *J. Mater. Res.* **1996**, *11*, 1581.
(11) Garnier, F.; Hajlaoui, R.; Yassar, A.; Srivastava, P. *Science* **1994**, *265*, 1684.
(12) Katz, H. E. *Chem. Mater.* **2004**, *16*, 4748.
(13) Kawase, T.; Shimoda, T.; Newsome, C.; Sirringhaus, H.; Friend, R. H. *Thin Solid Films* **2003**, *438−439*, 279.
(14) Chabinyc, M. L.; Toney, M. F.; Kline, R. J.; McCulloch, I.; Heeney, M. *J. Am. Chem. Soc.* **2007**, *129*, 3226.
(15) McCulloch, I.; Heeney, M.; Bailey, C.; Genevicius, K.; Macdonald, I.; Shkunov, M.; Sparrowe, D.; Tierney, S.; Wagner, R.; Zhang, W.; Chabinyc, M. L.; Kline, R. J.; McGehee, M. D.; Toney, M. F. *Nat. Mater.* **2006**, *5*, 328.
(16) Kline, R. J.; McGehee, M. D.; Toney, M. F. *Nat. Mater.* **2006**, *5*, 222.
(17) Ong, B. S.; Wu, Y.; Liu, P.; Gardner, S. *J. Am. Chem. Soc.* **2004**, *126*, 3378.
(18) Bao, Z.; Dodabalapur, A.; Lovinger, A. J. *Appl. Phys. Lett.* **1996**, *69*, 4108.
(19) Sirringhaus, H.; Brown, P. J.; Friend, R. H.; Nielsen, M. M.; Bechgaard, K.; Langeveld-Voss, B. M. W.; Spiering, A. J. H.; Janssen, R. A. J.; Meijer, E. W.; Herwig, P.; De Leeuw, D. M. *Nature (London)* **1999**, *401*, 685.
(20) Yang, H.; Shin, T. J.; Yang, L.; Cho, K.; Ryu, C. Y.; Bao, Z. *Adv. Funct. Mater.* **2005**, *15*, 671.

 10.1021/ja8095569 CCC: $40.75

their electrical performance decreases significantly, primarily due to the sensitivity of the polymer chains to atmospheric O_2/H_2O and to structural defects.[9,21] Channel materials need to have environmental and electrical reliability as well as a sufficiently low off-state current and a high charge-carrier mobility if they are to be used in high-resolution liquid crystal displays (LCDs) and organic light emitting diodes (OLEDs).[15,22−24]

In general, the oxidative stability of π-conjugated polymers depends on their ionization potential (IP), that is, on the energy of the highest occupied molecular orbital (HOMO) with respect to vacuum. New polythiophene derivatives with various classes of fused aromatic rings in the polymer backbone have recently been found to exhibit even higher charge mobility and oxidative stability than regioregular head-to-tail poly(3-hexylthiophene) HT-P3HT.[15,17,24] Electron-donating (p-type) thiophenes are the most commonly incorporated into polymer backbones, resulting in environmental and electrical stability limitations. This situation inspired us to design a polymer system with electron-accepting and electron-donating building blocks, that is, a donor−acceptor type alternating copolymer with liquid-crystalline nature, to optimize processability, crystalline nanostructure, and environmental/electrical reliability. It has recently been reported that π-conjugated polymers with donor−acceptor structure along the polymer main chain exhibit interesting electrochemical, optical, and electronic properties.[25−27] McCullough et al. have demonstrated that semiconducting polymers comprised of electron-accepting thiazolothiazole units in the polymer backbone have high charge mobility and enhanced oxidative stability.[28] However, they reported that these polymers exhibit less-ordered liquid-crystalline nanostructure because their long-range ordering is weaker than that of polythiophenes.[28]

Another common problem with OFETs is that they tend to exhibit some electrical instability under external bias stress, likely due to charge traps created through partial disorder in the structure of the thin films and the characteristics of the semiconductor/insulator interface. Bias-stress instability and environmental instability can be significant challenges for semiconducting polymers.[29−36] To be comparable to a-Si-based TFTs, OFETs should exhibit similar resilience with respect to electrical bias stress.[37] Although there have been a few studies aimed at enhancing the electrical stability of π-conjugated polymers under external bias stress, an adequate understanding of the relationship between crystalline nanostructure and bias stress driven electrical instability on the microscopic scale is still needed. Therefore, an in-depth and systematic study of highly ordered π-conjugated copolymer thin films with minimal concentration of charge traps is crucial.

Scheme 1. Synthetic Schemes for the Tetramer and the Corresponding Semiconducting Copolymer, **PQTBTz-C12**, Composed of Quaterthiophene and 5,5′-Bithiazole Units[a]

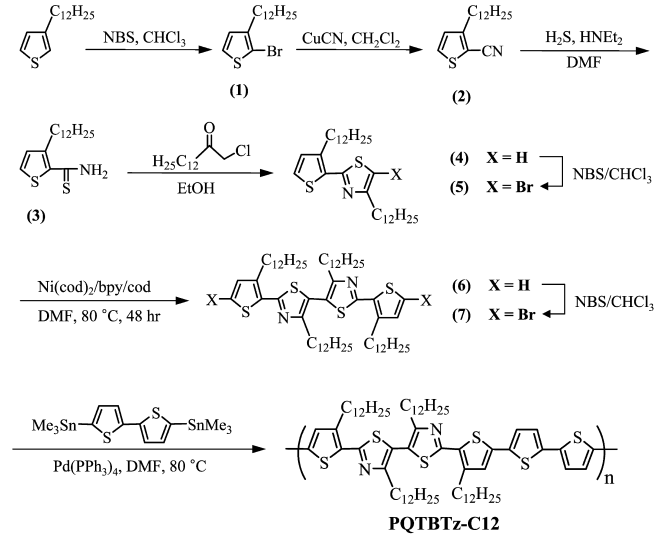

[a] NBS, *N*-bromosuccinimide; DMF, *N*,*N*-dimethylformamide; cod, 1,5-cyclooctadiene; bpy, 2,2′-bipyridine.

Here, we have designed a new donor−acceptor type copolymer (see Scheme 1), poly(didodecylquaterthiophene-*alt*-didodecylbithiazole), **PQTBTz-C12**, by copolymerization of electron-donating thiophene and electron-accepting thiazole units into the same polymer backbone to increase the IP. In this case, the introduction of unsubstituted bithiophene units (the insoluble component) enhances intermolecular $\pi-\pi$ stacking. Furthermore, alkyl chain-substituted thiophene/thiazole blocks (the soluble component) along the polymer backbone were used to increase the IP because of the enhanced rotational freedom along the backbone[15] (Figure S5) and the electron-accepting nature of the 5,5′-bithiazole units.[25−27] In particular, **PQTBTz-C12** presents a liquid-crystalline nature with a clear mesophase region, resulting in highly crystalline thin films forming spontaneously through the self-assembly of individual chains after thermal annealing. Also, we confirm that this novel polymer exhibits high field-effect mobilities of 0.33 $cm^2/V\cdot s$, good environmental stability, and unprecedented bias-stress stability comparable to that of a-Si.[37] Our findings therefore enable the realization of high-performance and high-stability polymer electronic devices, thus offering a promising protocol for the bottom-up assembly of new flexible electronics.

Results and Discussion

PQTBTz-C12 has a higher IP value (5.19 eV) than does head-to-tail (HT)-P3HT (4.9−5.0 eV) measured under identical conditions, which suggests that **PQTBTz-C12**-based OFETs are likely to have a low off-state current (nonoxidative state).

(21) Bao, Z.; Feng, Y.; Dodabalapur, A.; Raju, V. R.; Lovinger, A. J. *Chem. Mater.* **1997**, *9*, 1299.
(22) Sirringhaus, H.; Tessler, N.; Friend, R. H. *Science* **1998**, *280*, 1741.
(23) Ong, B. S.; Wu, Y.; Liu, P.; Murti, K. *Synth. Met.* **2004**, *142*, 49.
(24) Li, Y.; Wu, Y.; Liu, P.; Birau, M.; Pan, H.; Ong, B. S. *Adv. Mater.* **2006**, *18*, 3029.
(25) Yamamoto, T.; Arai, M.; Kokudo, H.; Sasaki, S. *Macromolecules* **2003**, *36*, 7986.
(26) Yamamoto, T.; Kokudo, H.; Kobashi, M.; Sakai, Y. *Chem. Mater.* **2004**, *16*, 4616.
(27) Kokudo, H.; Sato, T.; Yamamoto, T. *Macromolecules* **2006**, *39*, 3959.
(28) Osaka, I.; Sauvé, G.; Zhang, R.; Kowalewski, T.; McCullough, R. D. *Adv. Mater.* **2007**, *19*, 4160.
(29) Payne, M.; Parkin, S.; Anthony, J.; Kuo, C.; Jackson, T. *J. Am. Chem. Soc.* **2005**, *127*, 4986.
(30) Stingelin-Stutzmann, N.; Smits, E.; Wondergem, H.; Tanase, C.; Blom, P.; Smith, P.; de Leeuw, D. M. *Nat. Mater.* **2005**, *4*, 601.
(31) Mathijssen, S. G. J.; Cölle, M.; Gomes, H.; Smits, E. C. P.; de Boer, B.; McCulloch, I.; Bobbert, P. A.; de Leeuw, D. M. *Adv. Mater.* **2007**, *19*, 2785.
(32) Mathijssen, S. G. J.; Kemerink, M.; Sharma, A.; Cölle, M.; Bobbert, P. A.; Janssen, R. A. J.; de Leeuw, D. M. *Adv. Mater.* **2008**, *20*, 975.
(33) Street, R. A.; Chabinyc, M. L.; Endicott, F.; Ong, B. *J. Appl. Phys.* **2006**, *100*, 114518.
(34) Street, R. A.; Salleo, A.; Chabinyc, M. *Phys. Rev. B* **2003**, *68*, 085316.
(35) Salleo, A.; Street, R. A. *Phys. Rev. B* **2004**, *70*, 235324.
(36) Salleo, A.; Endicott, F.; Street, R. A. *Appl. Phys. Lett.* **2005**, *86*, 263505.
(37) Tsukada, T. In *Technology and Applications of Amorphous Silicon*; Street, R. A., Ed.; Springer-Verlag: Heidelberg, 2000; Vol. 37, p 49.

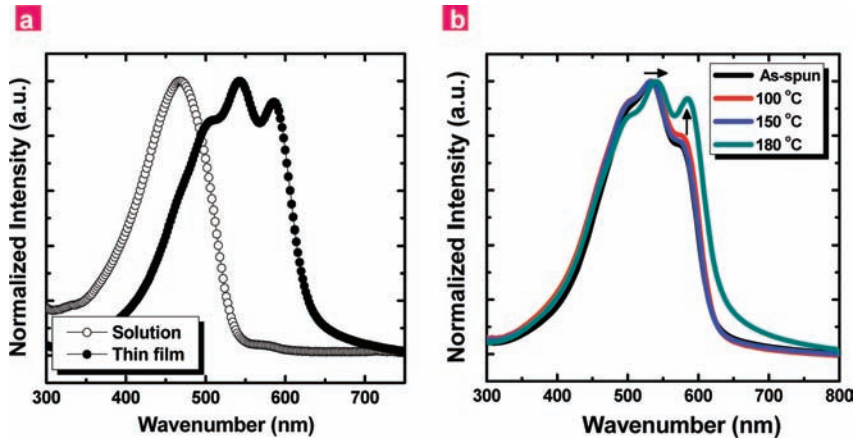

Figure 1. Phase and temperature dependences of the optical behavior of **PQTBTz-C12**. (a) UV−vis absorption spectra of **PQTBTz-C12** in solution (○) and thin film annealed at 180 °C (●). The large red-shift observed in the absorption maxima indicates that **PQTBTz-C12** self-assembles into a densely packed film. (b) Effects of varying the annealing temperature on the UV−vis absorption spectra of **PQTBTz-C12** thin films.

PQTBTz-C12 also exhibits high solubility in common organic solvents because of the presence of head-to-head (HH) linkages along the polymer backbone, which increases the twist angle between adjacent aromatic rings. Interestingly, devices fabricated with polymers with HH linkages usually exhibit low mobilities (ca. 10^{-4} $cm^2/V \cdot s$) because of both poor crystallinity and loose interchain interactions in the solid state;[25] however, **PQTBTz-C12** thin films were found to be highly crystalline, leading to high mobilities. The thermal properties of **PQTBTz-C12** were characterized with differential scanning calorimetry (DSC) (Figure S6). We found that **PQTBTz-C12** exhibits two discrete endotherm transitions ($T_{(S-M)h}$ and $T_{(M-I)h}$) on heating, and two exothermic transitions ($T_{(M-S)c}$ and $T_{(I-M)c}$) on cooling. The first transition corresponds to the solid−mesophase transition, and the second corresponds to the mesophase−isotropic transition. The DSC results suggest that the self-assembly of **PQTBTz-C12** should be significantly affected by thermal annealing. Interestingly, when the molecular weight of **PQTBTz-C12** was increased from 13KD to 22KD, the liquid-crystalline phase was weakened and finally became semicrystalline for a molecular weight of 41KD (Figure S7). We anticipate that varying the molecular weight of **PQTBTz-C12** will also affect its charge-carrier mobility and electrical instability under bias stress in OFETs as well as the crystalline microstructures.

The UV−vis absorption peaks of crystalline π-conjugated polymer films are usually shifted to longer wavelengths (red shift) relative to those measured in solution. This behavior is due to the intermolecular interactions between the polymer chains and the planarization effect of the π-conjugated polymer backbone, which enable the polymer chains to self-assemble into a well-ordered nanostructure in the solid state.[17,27,39,40] The extent of the red shift is related to the degree of order in the polymer;[27] for example, there is a large red shift (of more than 70 nm) for some regioregular π-conjugated polymers, such as HT-P3HT, whereas there is only a small shift or no shift at all for others, such as HH-P3HT.[39] In Figure 1, which shows the UV−vis absorption spectra of **PQTBTz-C12** in a chlorobenzene solution and in the solid state, the absorption peaks corresponding to the $\pi-\pi^*$ transitions of the polymer are present at 470 and 542 nm, respectively. This large red shift (of about 70 nm) suggests the presence of strong chain-to-chain interactions. **PQTBTz-C12** thin films exhibit a distinctive vibronic splitting with a strong shoulder near 584 nm, which is typical of regioregular semiconducting polymers.[17,27,39,40] In addition, the effects of thermal annealing on **PQTBTz-C12** films were investigated using UV−vis absorption spectra (Figure 1b). A 1 wt % chlorobenzene solution of **PQTBTz-C12** was spin-coated to fabricate films that were subsequently annealed at 100, 150, and 180 °C for 1 h under nitrogen. For the as-spun sample, the main absorption band of the **PQTBTz-C12** thin film is at 532 nm. Importantly, as the annealing temperature increased past 150 °C, the intensity of the 578 nm shoulder peak due to $\pi-\pi$ stacking as well as the main absorption band increased. These features became dramatically pronounced for samples annealed in the mesophase region (180 °C).

To investigate in detail the microstructure of the **PQTBTz-C12** thin films at different thermal annealing temperatures, we conducted grazing incidence angle X-ray diffraction (GIXRD)[8,14,41] and tapping-mode atomic force microscopy (TM-AFM) measurements. Figure 2a−c shows the two-dimensional (2D) GIXRD patterns of 60 nm **PQTBTz-C12** films spin-coated onto molecularly functionalized [octadecyltrimethoxysilane (OTS)-treated] SiO_2 substrates. By using a fixed grazing incidence angle (0.18°) that is above the critical angle for total reflection from the **PQTBTz-C12** thin films but below the critical angle (0.23°) of the SiO_2 substrate, the scattering from the substrate was reduced relative to the scattering from the films. In these 2D GIXRD patterns, intense (h00) crystal reflections with higher-order peaks (see the insets in Figure 2a−c), which can be used as a criterion for a lamellar stacking due to the alkyl side-chains along the a-axis (d-spacing of (100), $d_{(100)} = 21$ Å), are slightly scattered along the Debye rings in the q_z (out-of-plane) positions satisfying Bragg's law; this result suggests that most of the (h00) planes of **PQTBTz-C12** chains are oriented parallel to the gate dielectric (in the edge-on orientation). The 2D GIXRD patterns also contain two intense in-plane reflections appearing vertically at a given q_{xy} (>0), which can be indexed to (003) and (010). As shown in Figure 2a, in the case of the as-spun **PQTBTz-C12** thin films (i.e., not annealed), the 2D GIXRD pattern contains peaks with low

(38) Umeda, T.; Tokito, S.; Kumaki, D. *J. Appl. Phys.* **2007**, *101*, 054517.
(39) Chen, T. A.; Wu, X.; Rieke, R. D. *J. Am. Chem. Soc.* **1995**, *117*, 233.
(40) McCullough, R. D.; Tristram-Nagle, S.; Williams, S. P.; Lowe, R. D.; Jayaraman, M. *J. Am. Chem. Soc.* **1993**, *115*, 4910.
(41) Yuan, Q.; Mannsfeld, S. C. B.; Tang, M. L.; Toney, M. F.; Lüning, J.; Bao, Z. *J. Am. Chem. Soc.* **2008**, *130*, 3502.

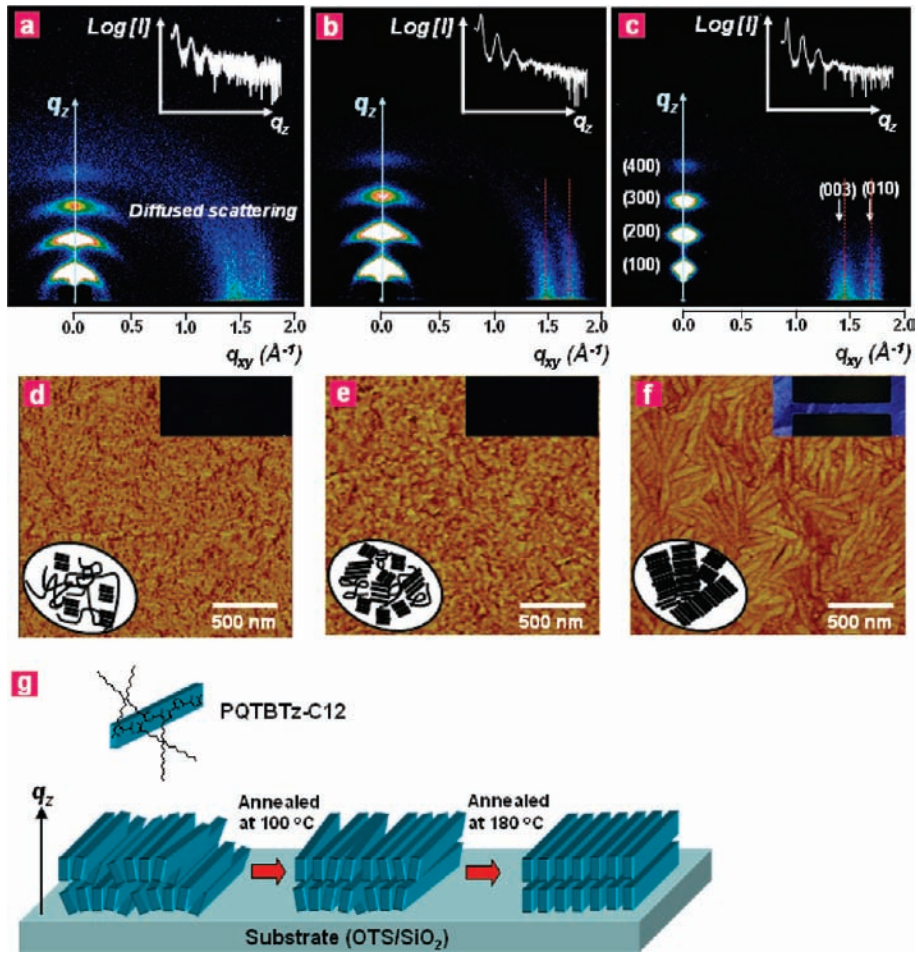

Figure 2. Effects of thermal annealing on molecular orientation and morphological features. 2D GIXD patterns of the **PQTBTz-C12** thin films spin-coated onto OTS-treated SiO_2 substrates for various annealing temperatures: (a) as-spun, (b) 100 °C, (c) 180 °C. The data are plotted versus the scattering vector q. (The insets in (a), (b), and (c) show the log-scale X-ray intensity profiles along the q_z axis, and the crystallographic assignments of the peaks are labeled.) AFM topographs of the **PQTBTz-C12** thin films spin-coated onto the OTS-treated SiO_2 substrates for various annealing temperatures: (d) as-spun, (e) 100 °C, (f) 180 °C. The insets in (d), (e), and (f) show the polarized optical microscope images (right-up) and schematic features of self-organization of the **PQTBTz-C12** chains for various annealing temperatures (left-down). (g) Schematic representation of liquid-crystalline domains in **PQTBTz-C12** thin films for various annealing temperatures, where q_z is the surface normal direction.

intensities and broadly diffused Debye rings of (h00), (003), and (010) reflections, implying low crystallinity and less-ordered crystalline nanostructure. The patterns for the samples annealed at 100 °C, which is below the observed solid−mesophase transition temperature, contain peaks with higher intensities (see the inset in Figure 2b) and split Debye rings of (003) and (010). On the other hand, for samples annealed at 180 °C, which is below the observed mesophase−isotropic transition (at mesophase), the patterns provide evidence of well-ordered molecular structure with perfectly edge-on orientation, in particular the narrow spots in the q_z (out-of-plane) direction (see Figure 2c). Further, the presence of distinctly vertical rod-shape patterns indicates that the **PQTBTz-C12** thin films consist of multistacked layers that are preferentially oriented normal to the substrate as well as to the lateral direction, although these in-plane GIXRD patterns also contain scattered reflections along the Debye rings. Furthermore, the azimuthal angle scan at the $q_{(100)}$ position (Figure S8) provides evidence that the polymer chains in the as-spun sample are less oriented relative to the substrate than the sample annealed at 180 °C, as shown in the schematic diagrams in Figure 2g.

High-resolution scans were used to determine precisely the d-spacings for **PQTBTz-C12** thin films to examine the degree of misorientation of the domains in greater detail. Enhancements in the intensity of the (h00) peak in the out-of-plane mode (Figure 3a) and the (010) peak in the in-plane mode (Figure 3b) occur with increased annealing temperature, which implies that the formation of liquid-crystalline domains with high out-of-plane and in-plane order is induced by thermal annealing. Further, when the angular spread of the orientations of the crystallites was measured, rocking curves on the (200) reflections were obtained (Figure 3c). We then imaged the Bragg scattering from the (200) peak to determine its relative misorientation with respect to the substrate over a wider range than possible with the high-resolution scans. Although the (200) peak is weaker than the (100) peak, the background scattering near it is significantly weaker than that at the (100) peak. The variation of the mosaic distributions in the **PQTBTz-C12** thin films can be measured because the rocking curve changes only the ω angle with respect to the Bragg angle when 2θ is on the Bragg reflection (the inset of Figure 3c). The mosaic distributions of the (200) crystal planes are almost unchanged by the annealing process, and only the number of well-oriented crystals is changed. In the case of the sample annealed at mesophase (180 °C), however, a sharp peak (with $|\omega| < 0.022°$) corresponding to well-oriented crystals appears, and the fwhm becomes as low as 0.04°. Interestingly, a broad background (with $|\omega| > 0.022°$),

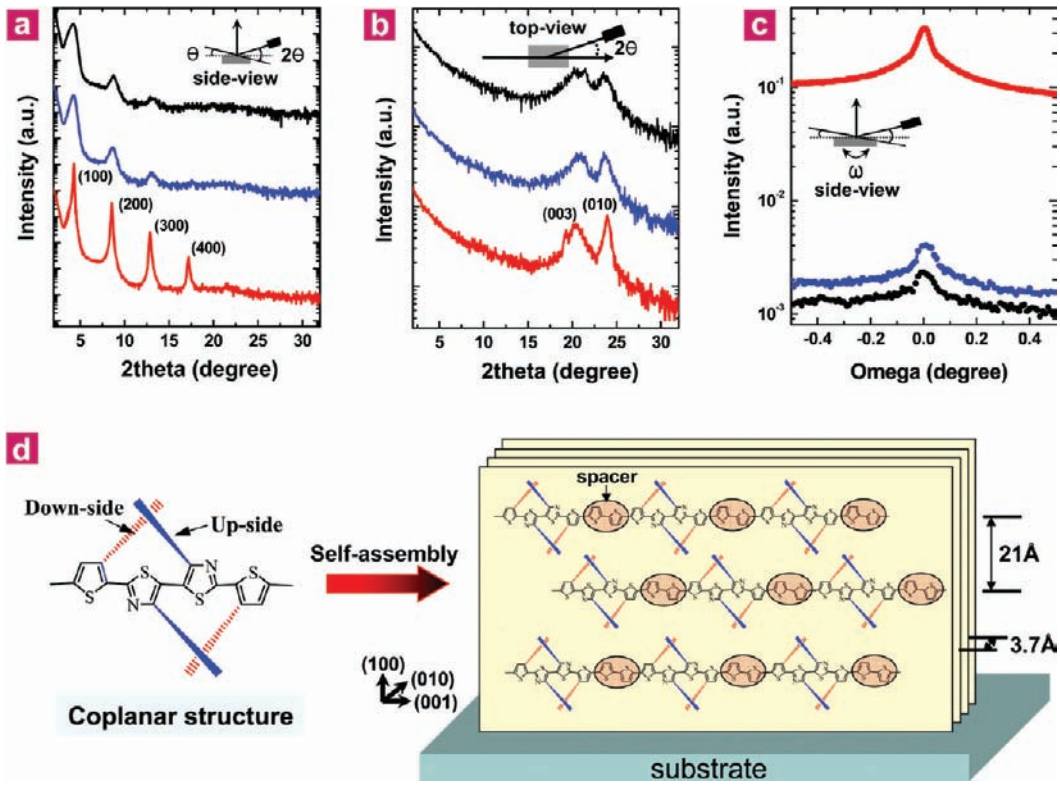

Figure 3. High-resolution X-ray scattering patterns of **PQTBTz-C12** thin films and their dependence on annealing temperature. (a) High-resolution specular X-ray scattering (out-of-plane), (b) grazing incidence X-ray scattering, and (c) rocking curves of the (200) peak for **PQTBTz-C12** thin films spin-coated onto OTS-treated SiO_2 substrates with various annealing temperatures. Black line, as-spun; blue line, annealed at 100 °C; and red line, annealed at 180 °C. The insets in (a), (b), and (c) show schematic diagrams of the geometry of the X-ray setup. (d) Schematic diagram of the self-assembly of the **PQTBTz-C12** chains on the specified surface, showing the edge-on orientation.

corresponding to marginally oriented crystals, is present as well, which might be due to the diffuse scattering induced by the increased roughness of the film (Figure 3c).[42] These results indicate that the lateral coherence length of the (200) planes increases with annealing temperature.[16] From these studies, we also can demonstrate that liquid-crystalline thin films form spontaneously through the self-assembly of the individual **PQTBTz-C12** chains as a result of intermolecular interactions in the liquid-crystalline mesophase and adopt preferential well-ordered intermolecular $\pi-\pi$ stacking (3.7 Å) parallel to the substrate surface (Figure 3d).

GIXRD measurements show the type of molecular structural order that is present within the **PQTBTz-C12** thin films, whereas the AFM observations can be used to determine the morphological features of the top surface. Figure 2d−f shows AFM phase images of **PQTBTz-C12** thin films prepared on OTS-treated SiO_2 substrates for various annealing temperatures. In the AFM images (Figure 2f) of **PQTBTz-C12** thin films annealed at the mesophase (at 180 °C), polycrystalline structures with rod-shape grains that are 300−500 nm in length are clearly evident, which arise from the self-organization of the **PQTBTz-C12** chains oriented perpendicularly to the substrates in the liquid-crystalline phase. This microscale morphology leads to the formation of highly ordered domains on the macroscale, giving rise to polarized optical microscopy (POM) findings (inset of Figure 2f) unlike those of the other samples (the insets in Figure 2d,e). However, as can be seen in Figure 2d and e, that is, for the sample annealed at 100 °C as well as the as-spun sample, nodule-like nanostructures with some nanofibers are observed, resulting from misorientation of **PQTBTz-C12** chains. The GIXRD, AFM, and POM results demonstrate that variations in the annealing conditions of **PQTBTz-C12** result in drastic changes in the molecular orientation, crystallinity, and surface morphology of its thin films. This ability to control the chain orientation and crystalline order enables us to establish later in this Article a direct correlation between the liquid-crystalline nanostructure and the electrical stability under external bias stress.

To determine the relationship between film morphology and electrical performance, the field-effect mobilities of **PQTBTz-C12** thin films in top-contact OFETs were measured. A cross-sectional view of the transistor device structure is shown in Figure 4a. The SiO_2 dielectric surface was modified with dense octadecyltrimethoxysilane (OTS) SAMs to enhance the electrical performance of the **PQTBTz-C12**-based OFETs. The SAM layers were determined to be molecularly flat over large areas by AFM with roughness around 0.2 nm. The detailed preparation procedure of this OTS SAMs is given in the experimental section in the Supporting Information. This OTS differs from most of those reported in literature in that it is a crystalline OTS characterized by GIXRD.[43] Such crystalline OTS layer was found to enhance two-dimensional growth for pentacene and resulted in higher charge-carrier mobility.[44,45] Figure 4b shows the typical output characteristics (I_D-V_D) at different gate

(42) Wölfing, B.; Theis-Bröhl, H.; Sutter, C.; Zabel, H. *J. Phys.: Condens. Matter* **1999**, *11*, 2669.

(43) Detailed characterization of this crystalline OTS is to appear in: Ito, Y.; Virkar, A.; Mannsfeld, S.; Tang, M.; Oh, J.; Locklin, J.; Toney, M.; Bao, Z., manuscript in preparation.

(44) Lee, H. S.; Kim, D. H.; Cho, J. H.; Hwang, M. K.; Jang, Y. S.; Cho, K. *J. Am. Chem. Soc.* **2008**, *130*, 10556.

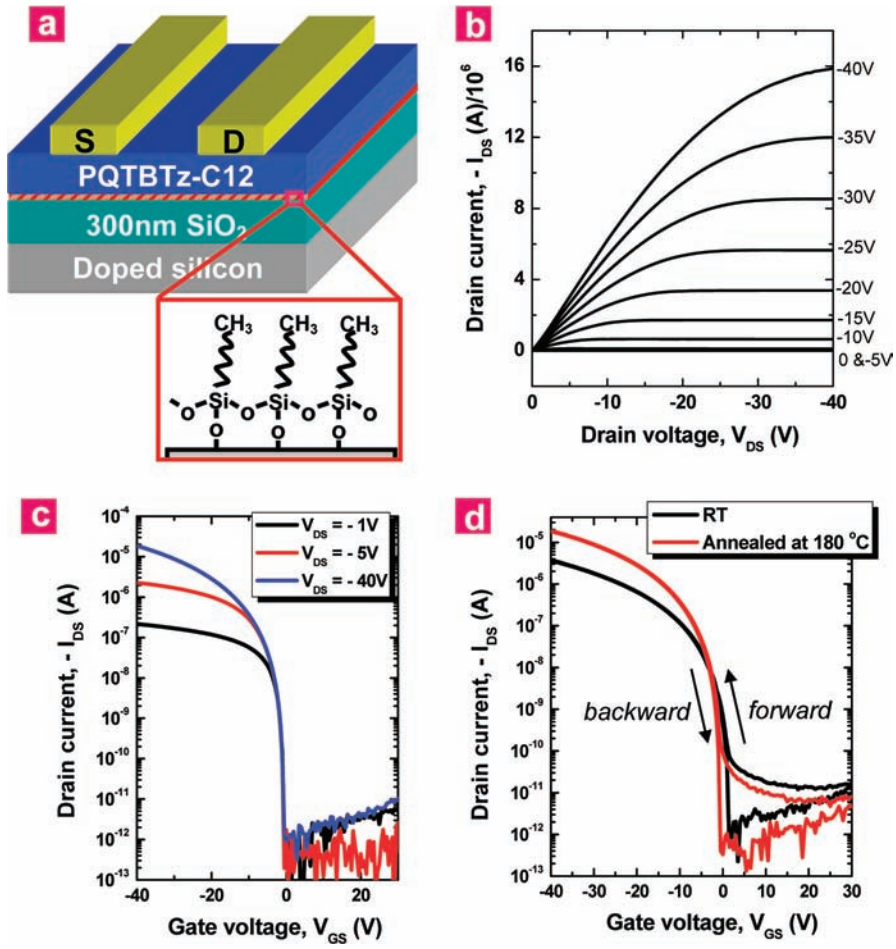

Figure 4. Performances of **PQTBTz-C12**-based OFETs and their variation with annealing temperature. (a) A schematic side-view of the transistor and a chemical representation of the OTS interlayer used in this study, (b) output (V_{GS}: 0 to −40 V), and (c) transfer characteristics of a device with $W = 1000$ μm and $L = 100$ μm based on the **PQTBTz-C12** thin film annealed at the mesophase (180 °C) for 1 h, exhibiting a field-effect mobility of 0.33 $cm^2/V \cdot s$ under ambient conditions. V_{DS} is the source-drain voltage, which was varied from −1 V (linear region) to −40 V (saturation region). (d) Comparison of forward and backward transfer plots according to annealing condition.

voltages (V_G) of OFETs based on **PQTBTz-C12** thin films annealed at the mesophase (180 °C) for 1 h. They are typical of p-type semiconductors, with well-resolved current linear regimes (ohmic region) in the low drain-source voltage range ($V_{DS} < -1$ V) and a saturation current near 16 μA at $V_G = -40$ V. Further, no significant hysteresis was observed (Figure 4d). By using the transfer characteristics of the transistors shown in Figure 4c, the average field-effect mobility (0.33 $cm^2/V \cdot s$) was calculated in the saturation regime ($V_{DS} = -40$ V) under ambient conditions.[46] In particular, a very low off-state current was observed (about 0.1−1 pA) as compared to the typical HT-P3HT system (about 10−100 pA). This result is explained by the deeper HOMO level (5.19 eV) of **PQTBTz-C12**, due to incorporation of electron-accepting units in the **PQTBTz-C12** backbone. In addition, we speculate that the decreased off-current can partly be a function of the highly crystalline nature of the SAM. Figure 5 shows the dependence of the average field-effect mobility on annealing temperature for devices on a 60 nm thick **PQTBTz-C12** film. Annealing the devices at the mesophase (180 °C) results in a field-effect mobility (0.33 cm^2 V^{-1} s^{-1}) that is about 1 order of magnitude higher than in the samples without annealing (0.04 cm^2 V^{-1} s^{-1}), although similar

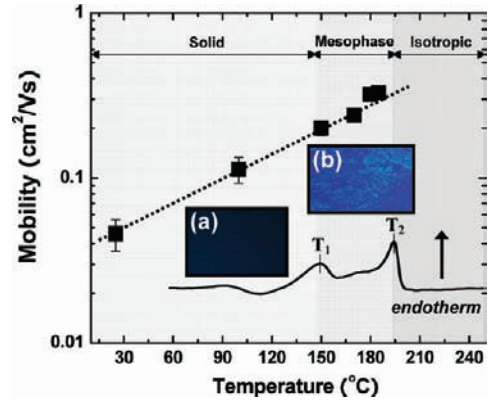

Figure 5. Variation in the charge-carrier mobility in **PQTBTz-C12**-based OFETs with annealing temperature. The inset shows the DSC curve, representing the liquid-crystalline mesophase and POM images of the samples annealed at (a) 100 °C and (b) 180 °C, respectively.

turn-on voltages are observed. Interestingly, the field-effect mobility is gradually modulated by the variation in annealing temperature, indicating that the vertically and laterally well-ordered crystalline phase in the **PQTBTz-C12** films promotes structural ordering, resulting in a high crystallinity and high field-effect mobility. In addition, as shown in Figure 6, **PQTBTz-C12** devices are more stable against atmospheric

(45) Virkar, A.; Mannsfeld, S. B. C.; Toney, M.; Tan, Y. H.; Liu, G.-Y.; Scott, J. C.; Miller, R.; Bao, Z., manuscript submitted.
(46) Horowitz, G. *Adv. Mater.* **1998**, *10*, 365.

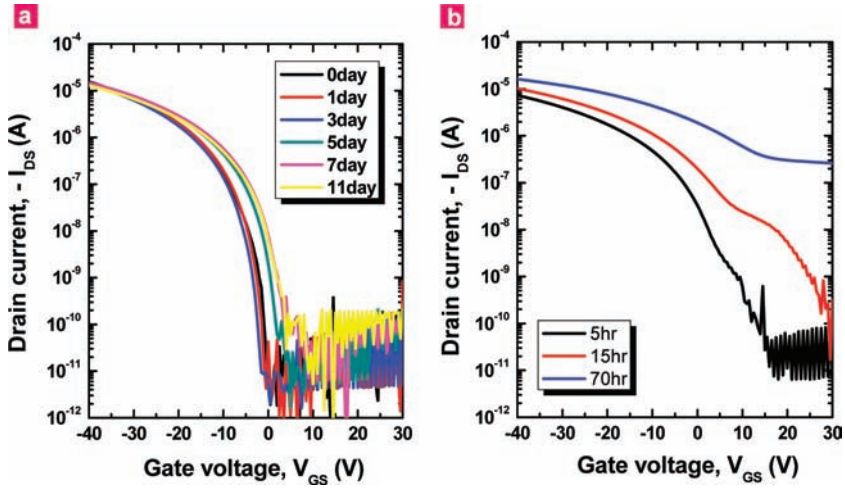

Figure 6. Air stability of (a) **PQTBTz-C12**-based and (b) P3HT-based OFETs.

oxygen than are P3HT-based devices, with only slight degradations in the mobility and the on/off ratio when they are stored under ambient conditions (humidity level $\approx$ 30%).[15]

The field-effect mobility of the **PQTBTz-C12**-based-OFETs is similar to that of the a-Si-based TFTs used in commercial display backplanes. However, if organic transistors are to replace a-Si TFT-based backplanes as the active elements in electronic devices, they should also exhibit excellent long-term electrical stability.[29−38] Unfortunately, OFETs commonly suffer from gate-bias or drain-bias stress under ambient conditions and over time cause a detrimental shift in the threshold voltage.[32] Such bias-stress instabilities, for example, charge-trapping instabilities, have been observed in OFETs for a wide range of materials, including pentacene,[47−50] various oligothiophene derivatives,[51,52] polytriarylamine,[31,32] polythiophene derivatives,[33−38,53] and polythienylenevinylene.[54,55] In an attempt to understand the physical origin of this charge-trapping instability, several studies have investigated this effect for various dielectric materials[56] and various dielectric surface treatments.[50,57] However, although important progress has been made in determining the charge-trapping mechanism in OFETs exhibiting electrical instability, no organic semiconductors with good electrical bias stability and high mobility have been reported. We now investigate the relationship between the film morphology and the charge-trapping instability of **PQTBTz-C12** on a hydrophobic molecular surface.

To determine the electrical stability of the **PQTBTz-C12**-based OFETs, a prolonged gate bias of −20 V was applied in ambient and inert conditions (under N_2) for 10 000 s (about 3 h), and its effects on the drain current and charge-carrier mobility were monitored. The transfer curves were measured at a drain bias of −1 V (linear region) and −40 V (saturation region, see Figures S9 and S10) by sweeping the gate bias from 40 to −40 V. The transfer curves shift with stress time in the direction of the applied gate bias, as shown in Figure 7a−c. Thus, a negative gate-bias stress causes a negative threshold shift, while the mobility remains unchanged. This effect is attributed to the shallow trapping of charges in less mobile states located in the semiconductor at the interface with the insulator.[49] In other words, the subthreshold slope of the device does not change even after the device has undergone gate-bias stressing, indicating that no additional defect states are created at the channel/insulator interface when the device is stressed.[58] The threshold voltage shift (ΔV_{th}) is indicative of charge-trapping instabilities in the transistor; that is, the applied gate potential is effectively screened by a build-up of trapped charges in the gate dielectric insulator or in the active layer itself.[59] Interestingly, we observed that the magnitude of the ΔV_{th} shift decreases with increasing annealing temperature, from −14.5 V (unannealed) to −2.6 V (annealed at 180 °C). In other words, the device annealed at 180 °C (mesophase) exhibits the lowest V_{th} shift (the highest electrical stability). These results indicate that high hole mobility and high crystalline films tend to have enhanced electrical stability due to a smaller number of hole trapping sites (annealed at the mesophase). Also, the ΔV_{th} shift can be affected by the characteristics of the OTS SAM such as crystallinity and surface energy. In our case, the OTS SAM showed a highly crystalline nature,[43,45] resulting in a reduced number of charge-trapping sites as compared to those observed on SAMs prepared by conventional dipping methods. To demonstrate the effect of the properties of the OTS SAMs on the TFT performance (mobility and electrical stability), we are going to compare our crystalline OTS SAMs to those prepared by the traditional method in due course.

To better understand the electrical stability of our devices, we modeled the change in threshold voltage using the following equation.

(47) Kawakami, D.; Yasutake, Y.; Nishizawa, H.; Majima, Y. *Jpn. J. Appl. Phys.* **2006**, *45*, L1127.
(48) Diallo, K.; Erouel, M.; Tardy, J.; André, E.; Garden, J.-L. *Appl. Phys. Lett.* **2007**, *91*, 183508.
(49) Knipp, D.; Street, R. A.; Völkel, A.; Ho, J. *J. Appl. Phys.* **2003**, *93*, 347.
(50) Suemori, K.; Uemura, S.; Yoshida, M.; Hoshino, S.; Takada, N.; Kodzasa, T.; Kamata, T. *Appl. Phys. Lett.* **2007**, *91*, 192112.
(51) Schoonveld, W. A.; Oosting, J. B.; Vrijmoeth, J.; Klapwijk, T. M. *Synth. Met.* **1999**, *101*, 608.
(52) Gomes, H. L.; Stallinga, P.; Dinelli, F.; Murgia, M.; Biscarni, F.; de Leeuw, D. M.; Muck, T.; Geurts, J.; Molenkamp, L. W.; Wagner, V. *Appl. Phys. Lett.* **2004**, *84*, 3184.
(53) Salleo, A.; Street, R. A. *J. Appl. Phys.* **2003**, *94*, 471.
(54) Brown, A. R.; Jarret, C. P.; de Leeuw, D. M.; Matters, M. *Synth. Met.* **1997**, *88*, 37.
(55) Zilker, S. J.; Detchverry, C.; Cantatore, E.; de Leeuw, D. M. *Appl. Phys. Lett.* **2001**, *79*, 1124.
(56) Ng, T. N.; Daniel, J. H.; Sambandan, S.; Arias, A.-C.; Chabinyc, M. L.; Street, R. A. *J. Appl. Phys.* **2008**, *103*, 044506.
(57) Ng, T. N.; Marohn, J. A.; Chabinyc, M. L. *J. Appl. Phys.* **2006**, *100*, 084505.
(58) Suresh, A.; Muth, J. F. *Appl. Phys. Lett.* **2008**, *92*, 033502.
(59) Powell, M. J.; Van Berkel, C.; Hughes, J. R. *Appl. Phys. Lett.* **1989**, *54*, 1323.

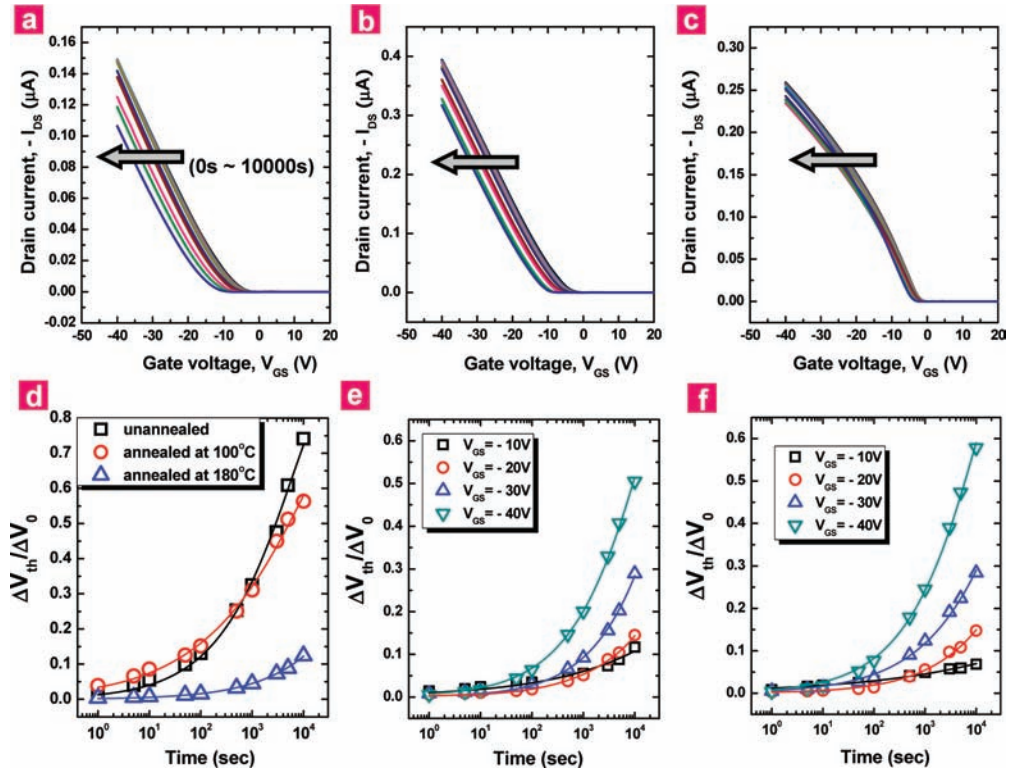

Figure 7. Threshold voltage shift (ΔV_{th}) under gate-bias stress and dependence of the charge-trapping instability on the liquid-crystalline nanostructure. Linear transfer curves of **PQTBTz-C12**-based OFETs as a function of stress time for various annealing temperatures: (a) as-spun (solid state), (b) annealed at 100 °C (solid state), and (c) annealed at 180 °C (mesophase). The gate bias during stress was fixed at −20 V, and the temperature under operation was room temperature (drain bias ≈ 0 V). The transfer curves were determined at a drain voltage of −1 V (linear region) and −40 V (saturation region, see Figure S9) by sweeping the gate bias from 40 to −40 V. (d) The relative threshold voltages ($V_{th}^{R} = \Delta V_{th}/\Delta V_0$) obtained from (a), (b), and (c) are presented as functions of stress time on a logarithmic scale. The solid curves are fits with a stretched-exponential time dependence: $\Delta V_{th}(t) = \Delta V_0(1 - \exp[-(t/\tau)^{\beta}])$. $V_0 = V_g - V_{th,0}$, where $V_{th,0}$ is the threshold voltage at the start of the experiment. ΔV_{th} is a function of stress time for various applied negative gate biases for sample annealed at 180 °C. (e) Drain voltage: −1 V (linear region). (f) Drain voltage: −40 V (saturation region).

There is a stretched-exponential decay in the threshold voltage with stress time:

$$\Delta V_{th}(t) = \Delta V_0(1 - \exp[-(t/\tau)^{\beta}]) \quad (1)$$

with $V_0 = V_g - V_{th,0}$, where $V_{th,0}$ is the threshold voltage at the start of the experiment. The relaxation time (τ) in eq 1 is thermally activated:

$$\tau = \nu^{-1} \exp(E_a/k_B T) \quad (2)$$

where E_a is the mean activation energy for charge trapping, and ν is a frequency prefactor. Figure 7d shows the relative threshold voltages ($V_{th}^{R} = \Delta V_{th}/\Delta V_0$: $V_0 = V_g - V_{th,0}$, where $V_{th,0}$ is the threshold voltage at the start of the experiment) as functions of stress time on a logarithmic scale. The solid curves are fits to this data with a stretched-exponential time dependence. The kinetics follow stretched-exponential time dependence behavior, in agreement with the formalism developed to explain metastability in a-Si-based TFTs.[60,61] By using this fitting model, it is possible to quantify the charge-trapping instability of the **PQTBTz-C12-**based OFETs. Remarkable agreement is observed in all devices for a relaxation time (τ) and a dispersion parameter (β), indicating that these two factors (τ and β) vary with the film microstructure, which affects the degree of interfacial trapping at the **PQTBTz-C12/OTS-SiO$_2$** interface.

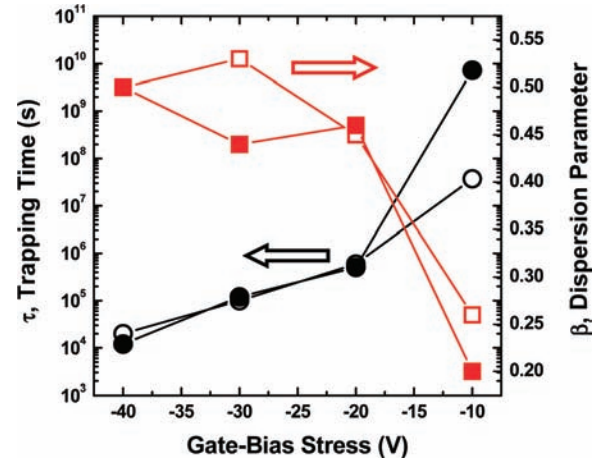

Figure 8. Dependence of the relaxation time (τ) and the dispersion parameter (β) on gate-bias stress for sample annealed at 180 °C. "○" and "□", determined at a drain voltage of −1 V (linear region); and "●" and "■", determined at a drain voltage of −40 V (saturation region).

Furthermore, Figures 7e,f and 8 show ΔV_{th} as a function of stress time for various applied negative gate biases and the dependence of the relaxation time (τ) and the dispersion parameter (β), respectively, on the gate bias. With increases in the gate-bias stress voltage, V_{th}^{R} effectively increases from 0.1 to 0.5, τ decreases from 5×10^7 to 2×10^4 s, and β increases from 0.2 to 0.5, which is similar to the case of a-Si-based TFTs, wherein β ranges from 0.2 to 0.3, indicating the dependence of charge-trapping instability on gate bias. The relaxation time (τ

(60) Wehrspohn, R.; Deane, S.; French, I.; Gale, I.; Hewett, J.; Powell, M.; Robertson, J. *J. Appl. Phys.* **2000**, *87*, 144.
(61) Wehrspohn, R.; Deane, S.; French, I.; Powell, M. *J. Non-Cryst. Solids* **2000**, *266*, 459.

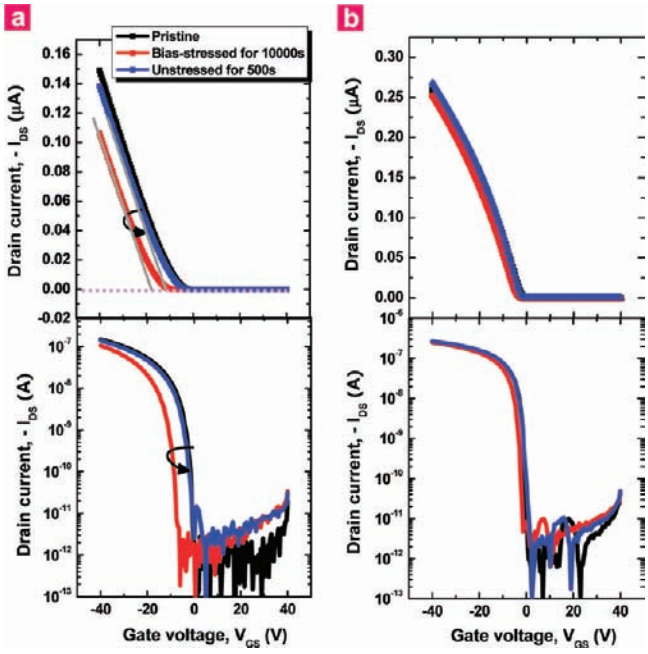

Figure 9. Recovery of ΔV_{th} via self-relaxation. Subsequent gate sweeps of devices annealed at room temperature (a) and 180 °C (b) under continuous gate-bias stress showing parallel shift along the gate voltage axis, plotted on linear and logarithmic scales of the channel current. After self-relaxation for 500 s, that is, once the stress is removed, the threshold voltages recover to their initial values.

$\approx 5 \times 10^7$) of **PQTBTz-C12**-based transistors is comparable to that ($\tau \approx 8 \times 10^7$) of a-Si-based TFTs.[31] However, there are other challenges in electrical instability of **PQTBTz-C12**-based transistors to be perfectly comparable to a-Si-based TFTs. These include off-bias driven instability and temperature dependency of electrical instability.

To examine the stress recovery phenomena, we compared the transfer curve during gate-bias stressing and after removal of the bias, and showed that after self-relaxation for 500 s, the threshold voltage recovers to its initial value irrespective of annealing conditions (Figure 9). This implies that charge-trapping instability is primarily generated at the near interface between polymer semiconductor and OTS-modified SiO_2 dielectric layer, not in the polymer bulk.

Conclusions

In conclusion, we have developed a novel, high performing, and highly stable donor−acceptor type liquid-crystalline semiconducting copolymer, **PQTBTz-C12**, by intramolecularly incorporating both electron-donating quaterthiophene and electron-accepting 5,5′-bithiazole units. This new polymer exhibits high field-effect mobilities of 0.33 $cm^2/V \cdot s$ and unprecedented bias-stress stability comparable to that of a-Si. Highly crystalline thin films are formed spontaneously after annealing through self-organization of individual polymer chains as a result of intermolecular interactions in the liquid-crystalline mesophase, which provides a facile means for the fabrication of a highly ordered semiconductor channel layer with a minimal concentration of charge traps and high electrical stability.

Acknowledgment. We gratefully acknowledge helpful technical support of atomic force microscopy by Ms. Y. Kwon in the AE group at SAIT and the Pohang Accelerator Laboratory for providing the 4C2, 8C1, and 10C1 beamlines used in this study.

Supporting Information Available: Experimental section; ^{1}H NMR spectra, FT-IR spectra, and DSC curves of **PQTBTz-C12**; UV−vis absorption spectra of **PBTBTz-C8** and **PQTBTz-C12** in the solid state; azimuthal angle scan at $q(100)$ position of **PQTBTz-C12** thin film according to annealing temperature; and linear transfer curves and the relative threshold voltages of **PQTBTz-C12**-based OFETs as a function of stress time for various annealing temperatures. This material is available free of charge via the Internet at http://pubs.acs.org.

JA8095569